Eur. Phys. J. B **11**, 665–676 (1999)

THE EUROPEAN PHYSICAL JOURNAL B

EDP Sciences

Corrective measures in turbulent pipe flows and extended self-similarity

M.S. Johansen, P. Alstrom, J. Borg, and M.T. Levinsen[a]

Center for Chaos and Turbulence Studies, The Niels Bohr Institute Blegdamsvej 17, 2100 Copenhagen Ø, Denmark

Received 5 August 1998 and Received in final form 21 December 1998

Abstract. Significant statistical bias in LDA measurements and how to adequately deal with it is a subtle problem when dealing with turbulent flows. In order to attempt a clarification we have performed measurements on a non-standard "grid experiment" where a clear bias effect is found. We have investigated the effect of several corrective measures and find that best results, in the sense of having the first moment converge to zero, are obtained when using the time between events as statistical weights. The corrected time series have been used to check for extended self-similarity (ESS). Even though no scaling regime is seen for the third moment and the flow certainly is neither isotropic nor homogeneous, perfect ESS scaling based on the absolute third moment is observed up to the twelfth moment, extending into a time domain regime where the Taylor hypothesis of frozen turbulence is obviously violated. Reversing the argument this indicates that the correction scheme needed can be experimentally decided on using the criterion stated above and especially so if ESS is to be expected. Finally we have used the corrected data to quantify the deviations from Gaussian behavior of the velocity difference probability density function for a weakly turbulent flow. Through comparison with results on the Gaussian-Lorentzian distribution we find that the even part of the experimental distribution can be reproduced quite well by a single-parameter family of distributions with second moment equal unity.

PACS. 42.79.Qx Range finders, remote sensing devices; laser Doppler velocimeters, SAR, and LIDAR – 47.80.+v Instrumentation for fluid dynamics – 47.27.-i Turbulent flows, convection, and heat transfer

1 Introduction

Even though the non-intrusive Laser Doppler Anemometry (LDA) technique for measuring fluid flow velocities has been around for quite a few years, it remains a difficult question how to deal with the problem of a significant bias in the datapoints acquired [1–7]. The LDA technique is based upon detecting light scattered from particles supposed to follow the flow. Thus obviously the datapoints are separated in time by intervals of random length determined by the spatial distance between scattering particles. The argument suggesting a bias effect is very simple. Under the assumption that the scattering particles are homogeneously distributed, in a non-stationary flow on the average more fluid and thus more particles per unit time will pass the measuring volume when the flow velocity is high than when it is low. If the scattering particles are not homogeneously distributed and especially if the particle distribution is itself correlated with the instantaneous velocity the problem gets even more complicated. Different schemes for dealing with the problem have been suggested and investigated by comparing with the result of extensive computer simulations. However, no all-embracing method has so far been developed.

[a] e-mail: levinsen@nbi.dk

Usually the statistical properties of a flow is studied by considering the distribution of velocity differences in two points over a given distance in space or time (the latter mostly being the case in experiments where the Taylor hypothesis of frozen turbulence is invoked if converting to space). These distributions are often explored through their moments and their variation with the distance separating the two points. Ideally one would like to have a signal that can be considered continuous on the time scale of typical velocity changes. However, with the LDA measurements this is normally not the case. Thus some interpolation scheme has to be involved in the treatment of time series. Compensation for eventual bias therefore includes a choice of an interpolation scheme together with a choice of how to weight the individual datapoints.

LDA measurements have been used extensively to study turbulent flows; also at high Reynolds numbers (Re), where the Kolmogorov theory of isotropic homogeneous turbulence (K41) [8] has a central place. The K41 theory seeks to predict the scaling behavior of the moments of the distribution of velocity differences, and much experimental work has gone into testing its validity. There is now general agreement that K41 does not give the correct scaling behavior for the moments, except for the third moment.

Turbulence at low Reynolds numbers has not received quite the same attention as high *Re* flows. A key notion in the K41 description is that turbulence is strong enough that small scales are well separated from the large injection scales. As the latter scales are determined by the details of the experiment, the presence of universal scaling behavior in low Reynolds number experiments is a question. In turbulence studies, the form of the velocity difference probability density functions (PDFs) $\rho(u)$ at different scales r is considered, as well as the moments, $\langle u(r)^n \rangle \equiv \int_{-\infty}^{\infty} u^n \rho(u) \mathrm{d}u$, or the absolute moments, $\langle |u(r)|^n \rangle \equiv \int_{-\infty}^{\infty} |u|^n \rho(u) \mathrm{d}u$. The moments are typically examined as a function of the scale r, in search for a possible scaling regime, where the moments follow a scaling law,

$$\langle |u(r)|^n \rangle \simeq c_n r^{\zeta_n} \ . \tag{1}$$

A new approach called Extended Self Similarity (ESS) has shown that it is possible to obtain *relative* scaling exponents at low Reynolds number by plotting moments of different order against each other in log-log plots instead of plotting them as a function of the separation r [9].

In order to study the validity of different correction schemes, we have applied them to time series obtained from a weakly turbulent flow created by placing a grid in a pipe flow. As a criterion for the best scheme we have used that the first structure function should be zero and that the third structure function should approach zero for large times (or distances). Having decided on the best scheme, we have then considered ESS. Intriguingly, we find that the data show perfect ESS even though the flow is far from what is traditionally considered a grid flow, the flow being spatially inhomogeneous due to a low number of grids. In some studies of ESS a scaling regime has been seen for the third moment, and the third and the absolute third moment are found to be proportional. Such a regime is completely absent in our measurements. Moreover, our measurements suggest that the correct moment to scale with in ESS is the absolute third moment, rather than the third moment. This is corroborated by a recent computer simulation [10]. One may speculate that ESS may be used as an instrument to check whether a proper correction for bias effects have been performed.

Due to the lack of analytical expressions for the form of the velocity difference probability density functions (PDFs) in turbulent fluids, a number of phenomenological models [11–17] have been suggested as useful approximations to the non-Gaussian shaped PDFs. The models have particularly been examined to account for the intermittent behavior in turbulent fluids [18] often related with the tails of the PDFs. In this paper, we are concerned with low *Re* flows, and therefore with the central deviations from the Gaussian behavior, rather than the tail structure. In order to examine the central part of the PDFs, we apply the two-parameter Gaussian-Lorentzian approximation to our experimental results. This method of quantifying the deviations from Gaussian behavior at low *Re* has previously been used to fit experiments attempting to check the Taylor hypothesis [19].

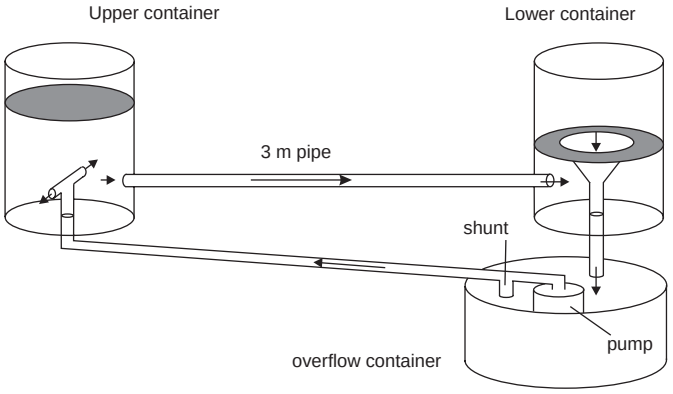

Fig. 1. Overview of the pressure driven flow experiment showing the water recirculation system.

Because the Gaussian-Lorentzian distribution is even, it can only be used as an approximation for the even part of the velocity difference PDF, and we shall only consider the absolute moments (the odd moments otherwise being zero). By rescaling velocities with the second moment we are left with a one-parameter family. As a surprising result of our analysis, the data obtained strongly suggest that a one-parameter (rescaled) family of PDF's (although not the Gaussian-Lorentzian distribution) may simulate the even part of the PDFs in the regime studied.

2 The grid flow experiment

2.1 The flow

A well known mechanism for generating homogeneous and isotropic turbulence is to place a grid in a laminar flow [20]. At high enough Reynolds numbers this will generate vortices of a size comparable to that of the rods in the grid. In the present experiment a grid consisting of four stainless steel rods (2 by 2 in parallel) is used as the turbulence generating obstacle. The grid is placed in a glass pipe of inner diameter 6 cm. The rods have a diameter of 10 mm and the spacing between the axes of the rods is 20 mm. This gives a solidity of the grid of 75%. The resulting flow is not what one traditionally characterizes as grid generated turbulence. For this the grid should consist of at least an order of magnitude more rods. However, we are here concerned with how to overcome possible biasing effects, and the possibility of ESS in an anisotropic and inhomogeneous case.

Nevertheless, we do want to be able to change the properties of the flow in a controlled way. The entrance section of the pipe is therefore filled with straws of diameter 6 mm and length 185 mm, in order to create a nearly laminar flow. As the length to diameter ratio is about 70, the velocity profile is still nearly flat at the outlet of the straws. After the straws the flat profile is maintained for the length of the pipe leading to the grid. The glass pipe consist of two 150 cm sections with the grid placed at the intersection. As the diameter of the straws is a factor of ten smaller than that of the pipe, so is the Reynolds

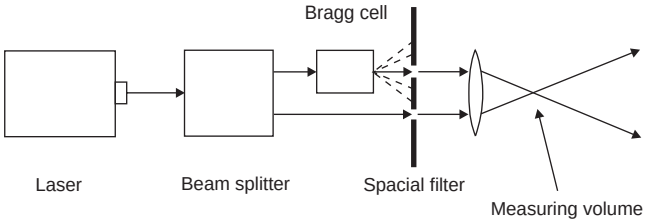

Fig. 2. Sketch of the optical system to produce the measuring volume.

number in the straws compared to that of the bare pipe. This lowering of the Reynolds number effectively kills the turbulence at the entry for the Reynolds numbers in the experiment.

The pipe is placed horizontally between two large containers each 65 cm in diameter and 90 cm in height. Figure 1 shows an overview of the feeding system. We use a pressure driven flow. Water is pumped from the lower reservoir container into the feed container by a Grundfoss model KP350-1 pump with a minimum capacity of 13.5 m^3 per hour. A shunt is used to regulate the pumping rate. The receiving container is fitted with an overflow funnel to keep the level constant. A valve at the outlet of the funnel gives a steady flow into the lower container to minimize the creation of bubbles by sloshing water. Even at the highest rate the water spends at least 30 seconds on the average in this container – enough for most visible bubbles to rize to the surface. As the visible bubbles are large (compared to the fringe spacing), they will destroy the quality of the Doppler signal rather than serve as scattering particles. The T-shaped entry into the feed container minimizes the amount of turbulence created in this container and no visible bubbles are present. The fluctuations of the surface in the feed container is of the order of 1 mm even with a flow velocity of 1 m/s in the pipe corresponding to a flow rate of close to 3 l/s. As the water level is about 60 cm at this rate, the fluctuations are less than 0.15% . The flow rate in the system could be adjusted by the shunt in the lower reservoir to within 0.01 m/s of a desired value. The stability of the mean flow is better than 0.3% per hour as checked by the time series obtained by the LDA system.

2.2 Optical part

The velocity was measured using a conventional LDA system based on the Dantec 58N20 correlation analyzer. A sketch of the optical setup is shown in Figure 2. The laser used is an Ion Laser Technology model 5500A, a 514.5 nm argon-ion laser with 200 mW output and 0.82 mm Gaussian beam diameter. The focusing lens has a 120 mm focal length and the measurements are done in the nearly-forward scattering mode. A rectangular box filled with water is placed around the pipe to minimize the optical distortion from the curved surface. The scattered signal is collected by an RCA 4536 photomultiplier tube. The Bragg cell could be driven by a fixed 40 MHz signal from the Dantec analyzer, but in these experiments a Philips

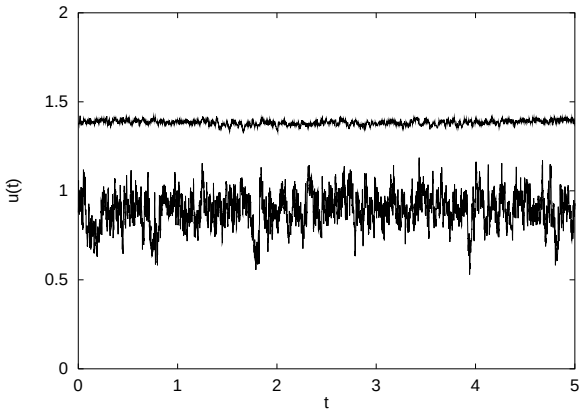

Fig. 3. Timeseries recorded just before the grid (upper trace and shifted upwards by 0.5 m/s) and 23 cm after the grid (lower trace).

PM 5193 synthesizer was used in order to tune the analyzer measuring window to better accommodate the signal bandwidth. The combination chosen was a compromise between obtaining the highest possible data rate (with a high validation) but retaining a velocity resolution better than 1%. With typical data rates around 1-2 kHz, a resolution of 1 μs for the arrival time was deemed sufficient.

In many applications of LDA the flow is seeded with small particles that act as scattering agents. In the present experiment this proved not to be necessary, probably due to the size and density of microscopic bubbles in the flow. By monitoring the burst envelope on an oscilloscope, it was easily verified that the distance between bursts compared with the width of the bursts would make it difficult to increase the density of scattering particles without at the same time increasing the probability of finding more than one particle in the scattering volume. This would result in a decrease of validation. It is a common experience that in recirculating flows it is often unnecessary to seed the flow as the bubbles naturally existing in the flow ensure a sufficient data rate [21].

2.3 The flow before the grid

As explained, some care has been taken to ensure that the flow is laminar before the grid. With a mean flow of 1 m/s the Reynolds number in the straw section is about 6 000. Thus the flow should be laminar. As the flow leaves this section the diameter changes by a factor of 10 and consequently the Reynolds number to 60 000. However, for the boundary created turbulence to reach the center of the pipe, the aspect ratio (length to diameter) should be of the order 50-100. In the present system the ratio is about 20, leading one to expect the flow still to be more or less laminar just before the grid. This was checked by making a comparison (at 1.03 m/s) between a time series taken just before the grid and one taken 23 cm downstream from the grid. The two time series are displayed in Figure 3 with the data taken before the grid displaced upwards by 0.5 m/s for clarity. It is clearly visible that the flow is

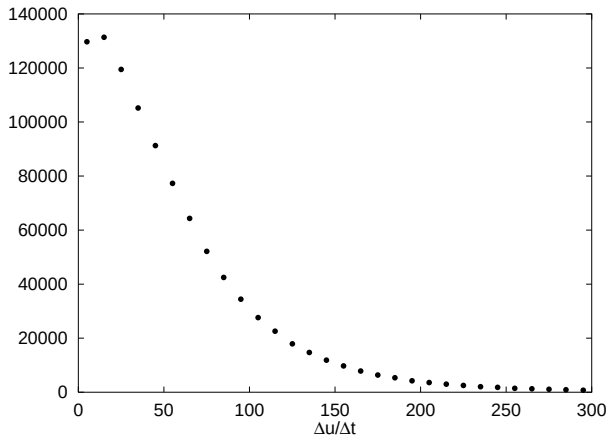

Fig. 4. Density of $\Delta u/\Delta t$.

much more turbulent after the grid and if not completely laminar before at least very close to. We therefore conclude that the relevant Reynolds number to use to characterize the flow is the one based on the diameter of the rods.

2.4 Velocity gradients

Measurements with the LDA technique are based on the assumption that the velocity of the scattering particle is constant during the crossing of the measuring volume. With turbulent flows this need not be the case, and one may suspect large fluctuations in the Doppler frequency to give imprecise measurements. We have no way to evaluate rapid small scale fluctuations, but on a larger scale the size of the fluctuations can be evaluated. In Figure 4 the PDF of the velocity time derivative $\Delta u/\Delta t$ is shown for the turbulent time series shown above in Figure 3. This is seen to have values up to 250 m/s^2 (99% is actually below this). With a mean transit time of 0.2 ms, this corresponds to a change in velocity of 0.05 m/s or a 5% change in frequency during the burst. From this we conclude that velocity changes during the transit of the measurement volume do not pose any problem.

All measurements in what follows are taken 23 cm downstream. The pressure difference was adjusted such that the mean flow velocity U in the center of the pipe varied between 40 and 105 cm/s. Thus, the Reynolds number $Re = Ud/v$ ($v = 0.01$ cm^2/s being the kinematic viscosity of water) lies between 4 000 and 10 500. Only the velocity component along the pipe axis was measured. The velocity difference PDFs were obtained from the data record as function of time; invoking the Taylor hypothesis, $r = Ut$, they may be turned into functions of space. The maximum turbulence intensity was about 10%. The data rate was about 1.5 kHz, and 60 min of data was recorded for each Reynolds number ($\sim 5 \times 10^6$ data points). In this connection let us mention that we have checked that the average velocity and turbulence intensity is constant across the tube except very close to the wall but the turbulence intensity is decaying significantly along the tube, the width of the velocity distribution being nearly halved at a further distance of 25 cm downstream.

3 Bias effects and methods of data analysis

3.1 The problem of statistical bias

As already mentioned above the argument suggesting a bias effect is very simple: Under the assumption that the scattering particles (whether they be seeding particles, bubbles or just dust) are homogeneously distributed in the liquid [22], in a non stationary flow one will experience a statistical bias due to the fact that on the average at high velocities more water and thereby more particles will flow through the measuring volume per unit time than at low velocities.

If the measuring volume is of size V and has the front area $A(\mathbf{v})$ perpendicular to the instantaneous direction of the flow, then the number of particles ΔN present in the volume that can provide a datapoint during the time Δt will be given by

$$\Delta N = \rho A(\mathbf{v}) v \Delta t. \tag{2}$$

Here ρ is the density of the scattering particles. Note that it is the size v of the instantaneous velocity $\mathbf{v}$ and not the measured component that enters into this expression. It is clear that the number of measurements is linearly dependent upon the three-dimensional velocity for a spherical measuring volume. In other words: in any time series there will be more (and more closely spaced) points at high velocities than at low. A simple average of these points will therefore give too high a mean value. For a non-spherical measuring volume the situation is more complicated, but a bias effect will still be present.

Based on the considerations above, McLaughlin and Tiedermann [23] suggested to use the measured component u as a statistical weight in the calculation of mean values. This is not without problems because one often lacks the spatial information that is necessary for a complete correction. McLaughlin and Tiedermann analysed a model where the measuring volume is spherical and the velocity fluctuations have a Gaussian distribution. With these assumptions numerical simulations show that the weighted sum is a good approximation to the real mean value. In actual cases the method works quite well for low intensity turbulence if more than one velocity component is known [3] even when the assumptions used in the original analysis are not met.

As indicated by equation (2) the data rate is to a first approximation linear in the velocity of the fluid as it passes through the measuring volume. As argued above it is the full three-dimensional velocity that is needed for a complete correction, but here we only have access to one of the components. The LDA analyser output, however, contains an additional parameter, the *transit time* (henceforth denoted t_T) which is ideally the time it takes the particle to travel through the measuring volume, and is estimated from the width of the Doppler burst. Weighting with the transit time is suggested by Buchhave *et al.* [1] who claims that the statistics are correctly produced with this weight. This method has since been proven to give good results by many experiments and computer simulations (see *e.g.* [4,5]) for all data rates.

In the above discussion, the data rate at the arrival time of particles plays a central role. It therefore seems interesting to use the instantaneous data rate as a statistical weight. If the data points are evenly spaced in time, the data rate is just the inverse of the time between particles. This method has also been extensively evaluated and shown to work if the data rate is high. Compared to the inverse integral time scale [2,3,5], in our experiments of the order of 100 Hz, our data rates are high (about 2 kHz).

However, other sources of bias can be present in a given experiment. Most relevant for a circulating flow is the question of non-homogeneous particle density. This becomes especially worrisome if the particle rate becomes dependent on the instantaneous velocity. The effect is treated in reference [2] and in detail in reference [5] through computer simulations. In reference [3] it is shown that weighting with the time between arrival most effectively removes the bias for all data rates, while weighting with the transit time on the other hand results in deviations that depend on the data rate and on the correlation (whether positive or negative) between the instantaneous velocity and particle rate.

To actually check whether a calculated average is in accordance with the true mean, some kind of calibration with respect to the given flow is required. This is not always easy or even possible, so here we shall employ another method to evaluate the different weighting methods.

Instead of focusing upon the mean value of the signal we shall use the velocity difference over the time τ,

$$\Delta u_\tau(t) = u(t) - u(t+\tau). \tag{3}$$

If this is averaged over time, it is identical to the first order structure function $S_1(\tau)$ which should disappear identically for all values of τ.

To see the effects of bias on the value of $S_1(\tau)$ we must consider how this is calculated in practice. Since the distance between data points is randomly distributed, it is in general quite unlikely that a data point will exist at time $t+\tau$ (or in a reasonably small neighborhood around it) if one exists at time t. One is then left with the choice of either skipping this point or constructing a data point by some interpolation scheme. Discarding the data is generally not desirable since as many points as possible are necessary in order to improve statistics. If the data rate is high enough to give an almost continuous time series, one could consider creating a smooth curve through the points close to the time where a data point is desired for instance by a cubic spline. With the data rate achieved in the present experiment, such an approach is unjustified.

We have considered three different interpolation schemes

- *linear interpolation* between the data points immediately before and after the time $t+\tau$. This amounts to approximating the real time series with a function that is piecewise linear between the data points;
- *sample and hold* where the value of the velocity is chosen as that of the last point before time $t+\tau$;
- *closest point* where the data point that is closest in time is used for the value of $u(t+\tau)$.

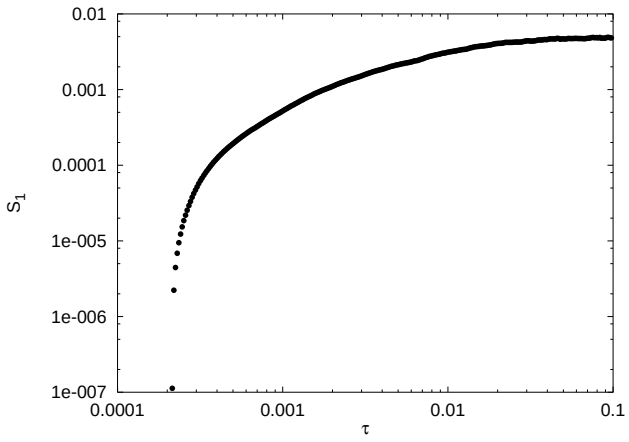

Fig. 5. The first order structure function $S_1(\tau)$ obtained experimentally without weighting data.

While these schemes all have obvious drawbacks we have settled on using the first since the bias only affects the starting point. In this way the continuous $\Delta u = u(t) - u(t+\tau)$ is replaced by the discrete $\Delta u_\tau(t_i) = u_{t_i} - u_{\rm int}(t_i+\tau)$ where t_i are the (discrete) arrival times of the particles, and $u_{\rm int}$ is the interpolated value. Now returning to the possible bias, it is important to note that this method of calculating $\Delta u(t)$ always uses an existing data point as the starting point. This will result in an overrepresentation of points with a high velocity. At a later time $t+\tau$ the flow will on the average have a higher possibility of a velocity, that is *lower* than at the starting point, since the velocity at $t+\tau$ is constructed by interpolation, and the expectation value of $u(t+\tau)$ therefore does not have any dependence of the data rate at time $t+\tau$. This leads to an overrepresentation of positive velocity differences, meaning that $S_1(\tau) = \langle \Delta u_\tau(t) \rangle$ will be positive if no corrective action is undertaken.

Figure 5 shows $S_1(\tau)$ calculated by a simple arithmetic mean,

$$S_1(\tau) = \frac{1}{N} \sum_i [u(t_i) - u_{\rm int}(t_i+\tau)], \tag{4}$$

i.e. without taking bias into account (N is the number of data points). It is evident that the first order structure function obtains a finite positive value, and for large τ a constant level is reached. This is in contrast with the requirement that $S_1 = 0$. Thus some degree of bias is truly present. The average flow velocity is 1.03 m/s, and a turbulent intensity of 10% is present, so typical fluctuations will be of the size of 0.1 m/s. Compared to this, the mean value of Δu_τ of 0.005 m/s (as seen from the graph) is significant. The interpolation scheme might as well use an existing data point as the end point and interpolate for the starting point. This will, for the reasons stated above, on the average lead to an overrepresentation of negative velocity differences. Even the first moment will therefore be different calculated by the two choices. The actual moments presented below are calculated as the mean of the moments obtained by the two choices, even though for clarity this is not explicitly stated in the following.

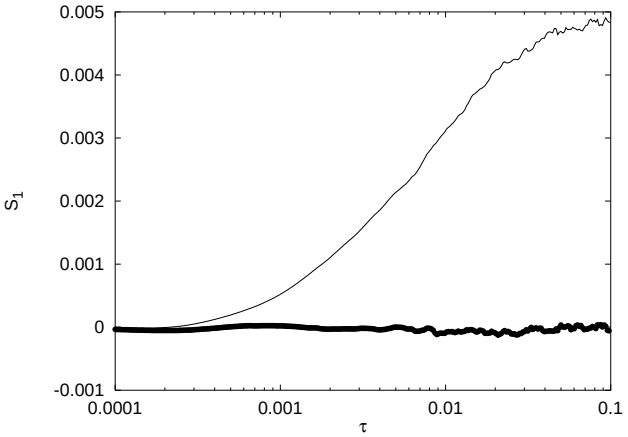

Fig. 6. $S_1(\tau)$ calculated with time-between-particles weight and without weight. The thin line is the unweighted values. The weighted values are shown by black dots. The time axis is logarithmic but S_1 is on linear scale.

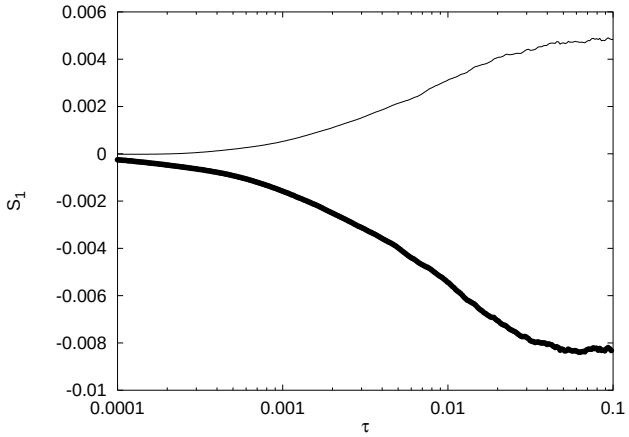

Fig. 7. S_1 with transit time weight (black circles) and without weight (thin line).

3.2 Weighting methods

Although the calculation of the first order structure function provides us with a way to check whether the statistics is biased, it does not provide us with a method to correct for the bias. Different schemes have been proposed, the most important being weighting with the time between samples and weighting with the time it takes the particle to cross the measuring volume as discussed above. Generally interest has centered on mean values such as the mean velocity, and it is often found (see *e.g.* [3]) that bias is present, but not significant. Here we concentrate on the moments, and even a small bias is significant.

3.2.1 Time between particles weight

As mentioned in Section 3.1, it seems interesting to use the instantaneous data rate as a statistical weight; if the data points are evenly spaced in time, the data rate is just the inverse of the time between particles. Of course the data are not evenly spaced but a good measure of the data rate is the inverse of $\Delta t_i = \frac{1}{2}(t_i - t_{i-1}) + \frac{1}{2}(t_{i+1} - t_i) = \frac{1}{2}(t_{i+1} - t_{i-1})$, *i.e.* half the time between the adjacent data points.

Using Δt_i as the statistical weight, we can then estimate the structure functions by

$$S_n(\tau) = \frac{\sum_i [u(t_i) - u_{int}(t_i + \tau)]^n \Delta t_i}{\sum_i \Delta t_i}, \qquad (5)$$

where u_{int} is constructed by the first interpolation method. Figure 6 shows $S_1(\tau)$ calculated by equation (5), and in comparison $S_1(\tau)$ calculated by equation (4) (Fig. 5), where bias is not taken into account.

In contrast to the unweighted values that approach a constant value for higher τ-values, the weighted values are zero with just small deviations oscillating around zero. This may be taken as a sign that the method works.

3.2.2 Transit time weight

From equation (2) we see that for a particle moving with velocity v the waiting time for the next particle to arrive is on average $(\rho A(\mathbf{v})v)^{-1}$. The product $A(\mathbf{v})v$ is proportional to the measured velocity component u. This suggests that the transit time $\Delta t_{\mathrm{T}} \sim u^{-1}$ is a relevant correction weight in calculating the moments. Figure 7 shows how $S_1(\tau)$ behaves compared to the unweighted estimate. It is seen that the use of the transit time weight does not move $S_1(\tau)$ closer to zero, as one would have expected. For our experimental situation, $S_1(\tau)$ is now negative and even further from zero than the unweighted moment. Although the transit time method has shown useful for other flows, the method is seen not to correct for the bias under our experimental conditions.

Another possibility is weighting with the overlap time where there are single particles simultaneously in *both* the volumes around time t_i and $t_i + \tau$ [1]. This is such a rare coincidence, that the method gives very poor statistics. Therefore it has not been possible to evaluate its potential in the present experiment.

3.2.3 Double time-between-particles weight

Both methods described above depend upon procedures used to constructing values by interpolation between actual data points. A different approach is to use actual data points as basis for the calculation. Here all available pair of points are used to compute their timeseparations $\tau_{ij} = t_i - t_j$. The corresponding products are then calculated, sorted into time lag bins, and the relevant moments calculated for each bin. A finite bin width will still introduce an interpolation error related to scheme 3. To minimize this error, the bin width has to be of the order of the average transit time. However, the number of Δu_τ values obtained in a given bin from a time series will be relatively low resulting in an increased scatter. Although choosing a larger bin width will make the graph look more smooth, this will affect the resolution of the τ-axis and increase the effect of the interpolation.

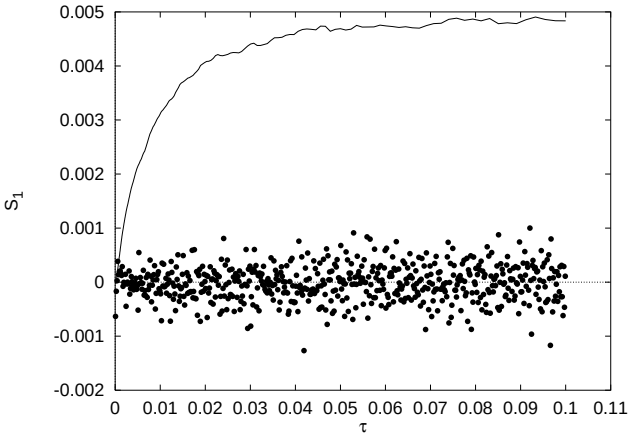

Fig. 8. S_1 calculated with the "double" time-between-particles weight.

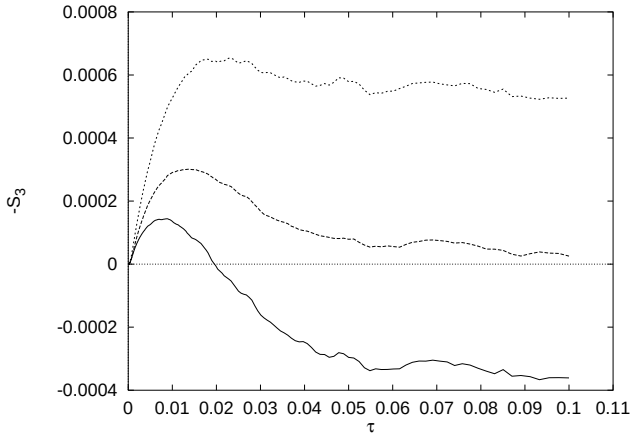

Fig. 9. Different weights applied to the calculation of S_3.

One has to adopt a different weighting, because now both points are affected by the overrepresentation of high velocities. Based on the results above, we have chosen to use the time-between-particles as the basis giving:

$$S_n(\tau) = \frac{\sum_{i,j}[u(t_i) - u(t_j)]^n \Delta t_i \Delta t_j}{\sum_{i,j} \Delta t_i \Delta t_j} \,. \qquad (6)$$

In Figure 8 the result for S_1 is shown together with the unweighted values. Note, that because the data is summed in bins of a fixed size, the τ-axis is now linear. The effect of this "double" weight is clearly to bring S_1 to the wanted zero value, but it is obvious that the data is much more scattered than was the case for the interpolated time-between-particles weight. This is only what one would expect on the basis of the reduced number of Δu values compared to the previous method and the effect of choosing the same small $\Delta\tau$ as in the previous analysis.

3.3 Comparison of the weighting methods

As the preceding sections show, the best method for correcting the statistical bias in the present experiment is by using the time-between-particles weight, which successfully gives $S_1(\tau) \approx 0$. This is supported by the "double" version, which although giving more scatter around zero has the advantage of being much less dependent on any interpolation scheme which could obscure the mechanism behind the correction. In Figure 9 is shown the result of the different weightings on the calculation of the 3rd order structure function. The three curves are clearly very different. The one at top is the unweighted value giving a positive finite value for larger τ. The lowest curve is calculated using the transit-time weight, giving a negative limiting value for large τ. In between these we find the result of the calculation using the time-between-particles weight falling nicely towards zero for large time differences. This is exactly the behaviour expected as the fluctuations for large separations must be uncorrelated giving a Gaussian distribution with all odd moments equal to zero.

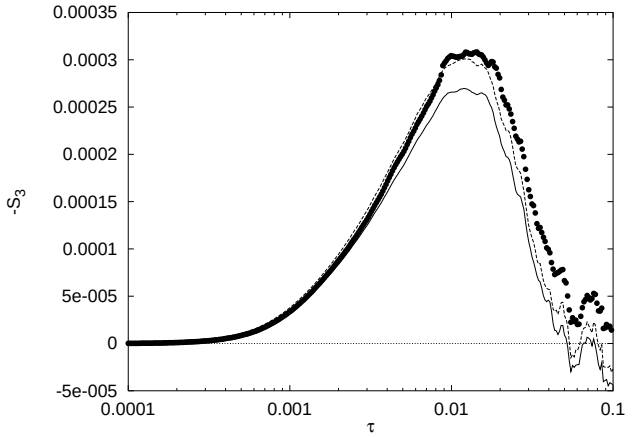

Fig. 10. Different weights applied to the calculation of S_3, using the central moments. Black circles are the time-between-particles data, the full line is the unweighted data, and the dashed line shows the transit-time weight data.

As the aforegoing shows, the weighting method has a significant effect on S_1 which should in theory be exactly zero, but in practice when weighting is taking into account fluctuates about zero. This suggests that it could be important to consider the central moments,

$$S_n(\tau) = \langle (\Delta u_\tau(t) - S_1(\tau))^n \rangle, \quad \text{for } n > 1. \qquad (7)$$

In Figure 10 the 3rd moment is shown calculated as central moments by subtracting the mean value S_1, as found by the respective methods, before raising to power 3. The black circles represent the values found by the time-between-particles weight. Rather closely following this we see the transit-time weighted data (dashed line) and below these (some 20% lower) is the unweighted data. It might seem tempting to conclude that the whole problem of bias is of little importance, as the different methods seem to give nearly the same result when applied to the central moments. This assertion is, however, not a trivial observation – it can only be made after having tested whether the data actually contains a significant bias. Also the 20% deviation in the third moment shows up as a rather noticeable larger deviation for the higher moments. It is,

however, reassuring that the statistics are robust to changing the weights when the central moments are considered.

An important time scale in the problem is the integral time scale,

$$T_{\rm int} \equiv \frac{\int_0^\infty {\rm d}t |\langle u'(t)u'(0)\rangle|}{\langle u'^2\rangle}, \qquad (8)$$

where $u'(t) = u(t) - \langle u(t)\rangle$.

In our case $T_{\rm int}$ is of the order of 10 ms. For the flow with mean velocity 1.03 m/s, the average sampling time is 0.54 ms. Thus the normalized data rate is approximately 20. According to reference [5], both the time-between-particles and the transit-time correction schemes should be able to correct for the bias if the seeding is homogeneous and no other sources of bias are present. However, from this study it seems clear that for a non-homogeneous seeding the method to employ is weighting with the time between arrivals. In the present experiments with a circulating flow, where bubbles are unavoidably created and participate as scattering particles, it might not be too unreasonable to expect the seeding to have a certain degree of non-homogeneity. Furthermore, one should note that as pointed out by Tiederman [24], the faster particles may have a smaller signal to noise ratio. This may result in underestimating the transit time thus leading to an overcompensation in the transit time correction scheme, while not affecting the time-between-particles method. A second source related to this may be the degrading of signal quality if particles are varying in size.

4 Extended self-similarity

In Figure 11 we display the numeric value of some of the higher moments calculated using the time-between-particle method discussed above for a mean flow velocity of U =1.03 m/s (the highest mean velocity obtained in the experiment). As expected for a regime of low to intermediate Reynolds numbers, we find no traces of any scaling regimes in Figure 11. Despite the fact that the flow is spatially inhomogeneous, we shall analyse our data looking for ESS by plotting the absolute structure functions $S_{|n|}$ *versus* $S_{|3|}$. These are defined using the absolute velocity differences in the equation (5) for the structure function S_n. The resulting plots are shown for two velocities (Reynold numbers of 10 300 and 5 800) in Figures 12 and 13. To make the data presentable in a single graph, the data is shifted so that the moments are plotted as $S_{|n|}/U^n$. This does not affect the slopes of the lines, it only changes their position. Also the data for Re = 10 300 are shifted up by a factor of 1.2, to be able to distinguish them from the Re = 5 800 data.

For $n = 2, 6, 7, 10$ the slopes obtained are shown as thick lines over the appropriate range. The values found (least-square fitting) are shown as ζ_n^* in Table 1. The quality of the scaling relation is rather good, *e.g.* S_2 as a function of $S_{|3|}$ (Fig. 14) deviates from a powerlaw by less than 0.3% in the range from 1 ms to 100 ms.

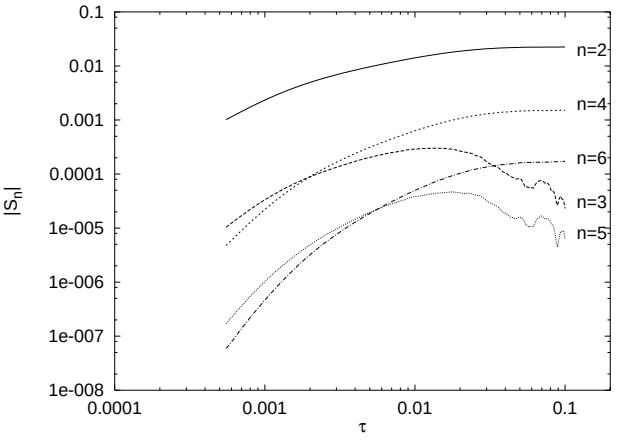

Fig. 11. S_n for $n = 2, 3, 4, 5, 6$ for Re =10 200.

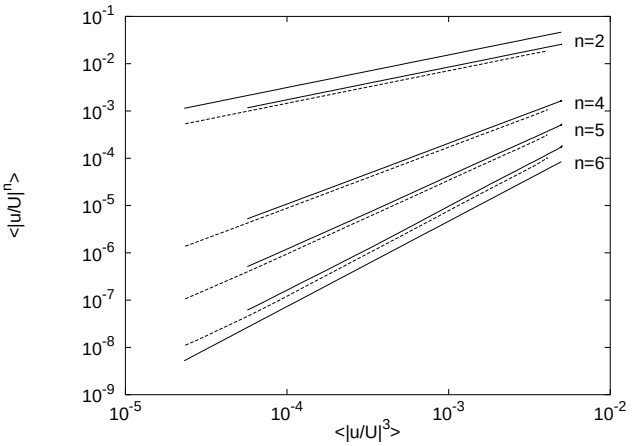

Fig. 12. The structure functions $S_{|n|}$ as a $S_{|3|}$ on double-logarithmic axis, for $n = 2, 4, 5, 6$. For $n = 2$ and $n = 6$ the slopes are shown as lines. Data is shifted as explained in the text.

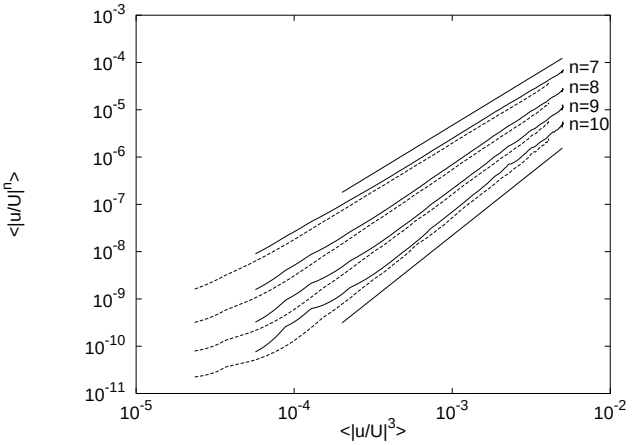

Fig. 13. As Figure 12, but for $n = 7, 8, 9, 10$.

For comparison, Table 1 also lists the values of ζ_n^* found by Benzi *et al.* [9]. The agreement is good, the difference being nowhere more than 2%. Also in the table are

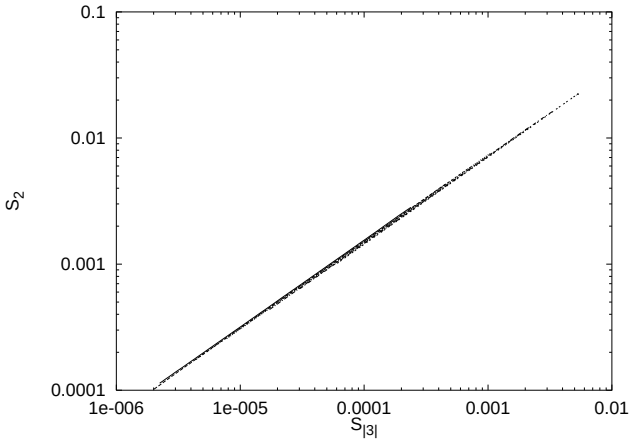

Fig. 14. S_2 *versus* $S_{|3|}$ for 7 velocities, plotted without rescaling.

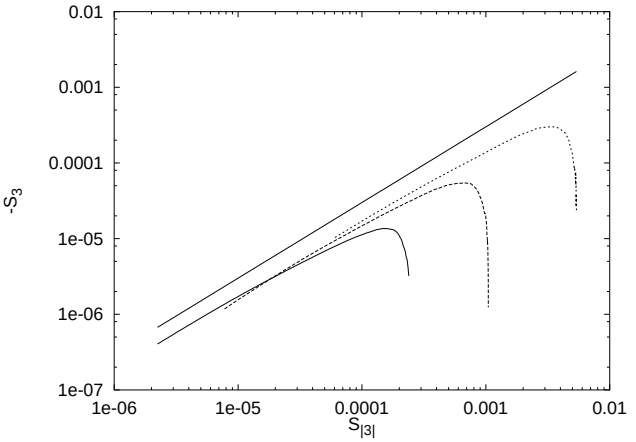

Fig. 15. The 3rd order structure function *versus* the absolute ditto. The line indicates the proportionality found in [9].

the data of a low Re experiment by Esposito *et al.* [25] in a pipe flow without a grid, and with measurements taken 100 diameters downstream.

A quantity often used to characterize flows is the Taylor-scale based Reynolds number

$$Re_{\mathrm{Taylor}} = \frac{\langle (u(t))^2 \rangle \lambda_{\mathrm{Taylor}}}{\nu}, \tag{9}$$

with the Taylor microscale $\lambda_{\mathrm{Taylor}}$ defined by

$$\frac{1}{\lambda^2_{\mathrm{Taylor}}} = \frac{\langle (\partial u(t)/\partial x)^2 \rangle}{\langle (u(t))^2 \rangle}\,. \tag{10}$$

The Taylor microscale can be determined directly by discretizing the definition and is found to be 1.3 mm for the flow velocity of 1.03 m/s quoted above. In our experiment Re_{Taylor} ranged from 60−140 compared to the value of ≈10 in the experiment by Esposito *et al.* [25].

Extended self similarity as found by Benzi *et al.* leans on the observation that S_3 and $S_{|3|}$ are proportional over the range where the relative scaling is found. In Figure 15 the relation between these values are shown, as found in the experiment. It is easily seen, that the individual graphs

Table 1. Scaling parameters obtained compared to those of Benzi *et al.* and Esposito *et al.* The uncertainty on our data is on the last decimal as estimated from the quality of the fit by manually varying ζ_n^*, since the uncertainties reported by the fitting routine were unrealistically low.

n	ζ_n^*	Benzi *et al.*	Esposito *et al.*
2	0.690 ± 0.001	0.70	0.690 ± 0.001
3	1	1	1
4	1.288 ± 0.001	1.28	1.296 ± 0.001
5	1.555 ± 0.005	1.54	
6	1.80 ± 0.01	1.78	1.819 ± 0.005
7	2.04 ± 0.02	2.00	
8	2.25 ± 0.02	2.23	2.22 ± 0.02
9	2.46 ± 0.03		
10	2.65 ± 0.05		2.60 ± 0.03
11	2.8 ± 0.1		
12	3.0 ± 0.1		2.95 ± 0.05

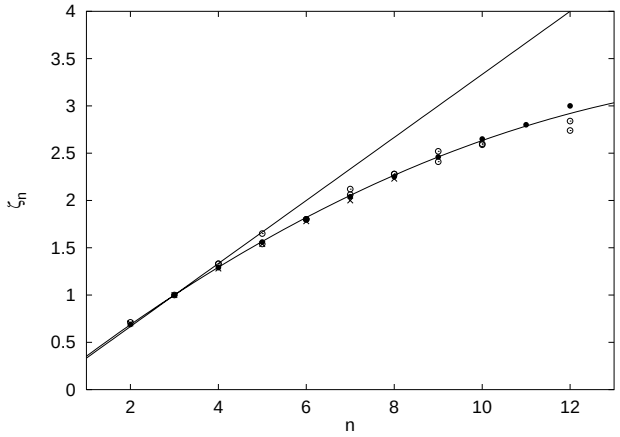

Fig. 16. The exponent ζ_n^* as a function of n. Black circles are ESS values from the experiment. Crosses are ESS values from [9] and ⊙ are from [26]. Straight line is K41, parabolic K62 with $k = 0.02$.

show no such proportionality (or power-law behavior). For lower values of $S_{|3|}$ (corresponding to small τ) they approach a slope of 1 (shown by a fat line in the figure). For higher values the graphs dip down towards zero in accordance with the PDF being found to be Gaussian for large τ (see the following section). Taken together though, the *envelope* of the individual graphs has a slope of 1.

The slopes given in Table 1 are clearly different from the trivial values $n/3$. The values are illustrated in Figure 16, and compared to those found by Benzi *et al.* [9]. Also shown in the figure are data by Anselmet *et al.* [26]. The straight line is the K41 $n/3$ result. The parabolic curve is the prediction by Obukhov and Kolmogorov [11,12] with $k = 0.02$, which is the value obtained inserting $\zeta_2 = 0.69$ in $\zeta_2 = 2/3 + k$ [12].

5 Distributions

Having established that the flow does possess scaling in the ESS-sense, we shall now consider the distributions themselves. Many models have been suggested as approximations to the velocity difference probability density functions (PDF's) for turbulent flows [11–17]. Here we shall investigate to what extent a two-parameter family of distributions is able to model the (weakly) turbulent state. One such family relevant for quantifying the deviations from Gaussian behavior is the Gaussian-Lorentzian (GL) distribution [19]. (In what follows u has been substituted for Δu for convenience). In this the velocity difference distribution $\rho(u)$ is expressed as a product of a Gaussian distribution, $\rho_{\rm G}(u) \propto \exp[-(u/u_{\rm G})^2]$, and a Lorentzian distribution, $\rho_{\rm L}(u) \propto [u^2 + u_{\rm L}^2]^{-1}$,

$$\rho(u) = N \frac{\exp[-(u/u_{\rm G})^2]}{u^2 + u_{\rm L}^2} \ . \qquad (11)$$

In the above expression $u_{\rm L} = u_{\rm L}(r)$ and $u_{\rm G} = u_{\rm G}(r)$ are the characteristic velocities for the two distributions for a given distance r, and N is a normalization constant assuring that $\int_{-\infty}^{\infty} \rho(u) {\rm d}u = 1$. The Gaussian-Lorentzian distribution is an even function. This means that it can only be used as an approximation for the even part of the velocity difference PDF, and we shall return to this point below. First, however, we shall consider the quality of the fit between experimental PDF's and the GL distribution.

5.1 Quality of the fit

The chosen method of fitting is least squares on linear scale. This has shown to give the best convergence of the fit. Fitting the logarithm gave essentially the same results, but was more sensitive to small fluctuations in the tail of the PDF.

First we shall consider how well the even part of the PDF is actually described by the GL-approximation. In Figure 17 the even part of the experimental PDF and the corresponding GL-fit is shown for three different values of τ: 0.3 ms, 1 ms, and 10 ms for the flow with mean velocity of 1 m/s, but the quality is the same for all velocities. In these fits the velocity difference u is scaled with the second moment ($u \to u' = u/\langle u^2 \rangle^{1/2}$). For all three τ values, the fit is seen to be very good. In fact $\tau = 0.3$ ms is below the mean separation between data points in the time series (which is 0.5 ms), so we conclude that the GL-fit is a good approximation to the central part of the PDF for time-scales which can be resolved in the experiment. For $\tau >$10 ms the PDF is still well described by the GL-fit, as it rapidly becomes indistinguishable from a Gaussian.

If the same data is plotted semi-logarithmically to emphasize the tails (see Fig. 18), it is seen that the GL-fit is good up to $u' = 3$, (corresponding to 3 times the variance in the unscaled PDF). For larger values the fit is no longer good, underestimating the tails, as the Gaussian part inevitably ends up dominating. We conclude that the Gaussian-Lorentzian approximation is a good fit to the centre of the even part of the velocity differences PDF. The tails are not described by the model.

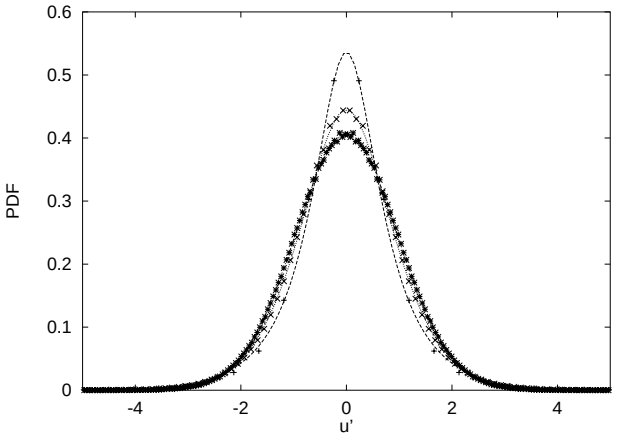

Fig. 17. PDF and GL-fit for three τ values (0.3 ms, 1 ms and 10 ms). For higher τ the PDF approaches a Gaussian.

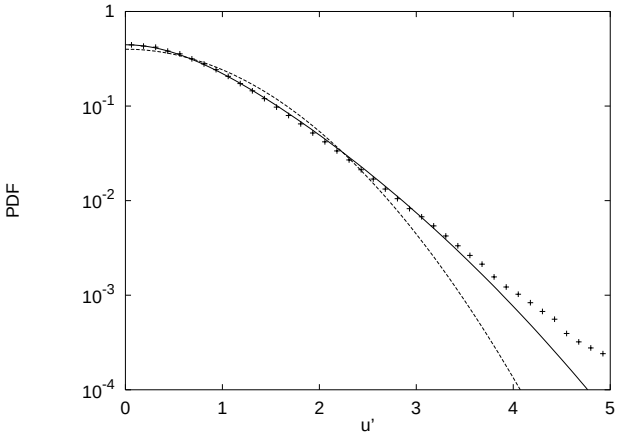

Fig. 18. Data for τ= 1 ms but now plotted semilogarithmic.

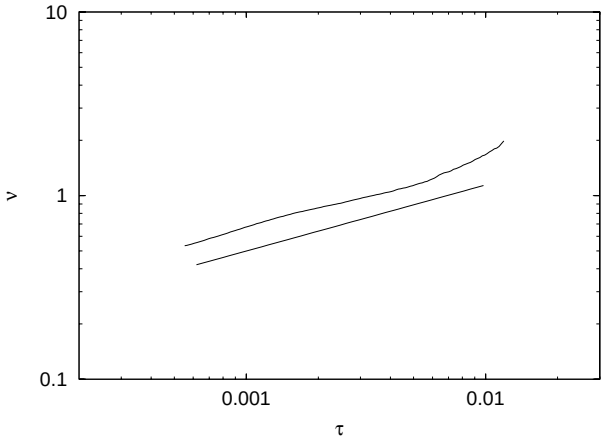

Fig. 19. A double logarithmic plot of ν as a function τ. The thick line has a slope of 0.36. The Reynolds number is 10300. The dashed line is an extrapolation of the approximate power law.

The parameter describing the change in the GL distribution is the ratio $\nu(\tau) = u_{\rm L}/u_{\rm G}$ [19]. In Figure 19

this relationship is plotted for $Re = 10\,300$, but no change in the curve is noticed with the change in Reynolds number obtained in this experiment. The curve $\nu(\tau)$ approximately follows a power-law,

$$\nu(\tau) \propto \tau^{0.36}, \tag{12}$$

for τ in the range 0.5 to 10 ms. In this range ν changes from 0.5 to 1.5. For larger values of τ the PDF is so close to being Gaussian that the experimental noise makes a distinction meaningless.

5.2 Moments

The (absolute) moments for the Gaussian-Lorentzian distribution function (11) has the following form,

$$\langle |u(r)|^n \rangle = N \int_{-\infty}^{\infty} \frac{|u|^n \exp[-(u/u_{\mathrm{G}}(r))^2]}{u^2 + u_{\mathrm{L}}(r)^2} \mathrm{d}u$$
$$= N u_{\mathrm{L}}^{n-1} \exp[\nu(r)^2] \Gamma\left(\frac{n+1}{2}\right) \Gamma\left(\frac{1-n}{2}, \nu(r)^2\right). \tag{13}$$

In the above formula $\Gamma(\alpha) = \int_0^\infty \mathrm{e}^{-t} t^{\alpha-1} \mathrm{d}t$ is the Γ-function, and $\Gamma(\alpha, x) = \int_x^\infty \mathrm{e}^{-t} t^{\alpha-1} \mathrm{d}t$ is the incomplete Γ-function [27,28]. The normalization constant N can be determined by setting $n = 0$.

In rescaled units we find

$$\langle |u'|^n \rangle = \left(\frac{2\Gamma(1/2, \nu^2)}{\Gamma(-1/2, \nu^2)}\right)^{n/2} \frac{\Gamma\left(\frac{n+1}{2}\right)}{\Gamma(1/2)} \frac{\Gamma\left(\frac{1-n}{2}, \nu^2\right)}{\Gamma(1/2, \nu^2)}. \tag{14}$$

By definition $\langle |u'|^2 \rangle = 1$. The other moments are functions only of the single parameter ν.

In Figure 20 the rescaled moments $\langle |u'|^n \rangle$ for $n = 3$, 4, and 6 are shown *versus* ν. The lines correspond to the moments of the GL model, while the experimental data plotted as points are for Reynolds numbers 10300 and 5800. The 3rd moment shows overall fine agreement, whereas the 4th and the 6th moments show increasing discrepancy for decreasing values of ν (corresponding to the Lorentzian dominated regime of the PDF). This is caused by the failure of the Gaussian-Lorentzian distribution to fit the tails of the experimental distributions.

The GL model distribution does not give a very good fit to the tails. However, it is a remarkable fact that the experimental data for all the moments, within experimental uncertainty, fall on unique curves, independent of Reynolds number. This shows that the even part of the velocity difference distributions in terms of the rescaled velocity u' at least is very close to be determined by a single parameter. In Figure 20 this parameter is taken to be ν, but the parameter used could equally well be one of the moments (aside from the unit second moment), for example the third moment, thus again connecting to extended self-similarity.

To account for the skewness observed in experimental data, at least a second parameter is needed.

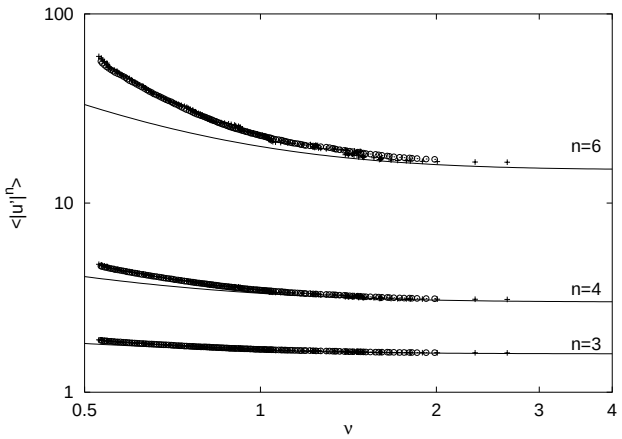

Fig. 20. The moments $\langle |u'|^n \rangle$ in a double-logarithmic plot *versus* ν for $n = 3, 4, 6$. Also the experimentally obtained moments are plotted for $Re = 5\,800$ (+) and $Re = 10\,300$ (∘).

6 Conclusions

An experiment has been performed on a non-standard grid-flow at intermediate Reynolds numbers (4 000-10 000). Laser Doppler Anemometer generated time-series of flow velocities were found to possess a significant bias. Such a bias can result from many different causes, both involving the flow and the electronics.

In many cases a complete control over experimental parameters is not possible and the correct procedure to follow to remove the bias therefore not obvious. Using the criterion that the first moment should in principle be zero, we have investigated several corrective procedures and find that for our experiments a very good result is obtained by weighting with the time between sampled points.

Using this corrective scheme we have looked for extended self-similarity in the data. However, not entirely unexpected with such low Reynolds numbers and a flow that is not homogeneous and isotropic, we do not see any proportionality between the 3rd order structure function and the 3rd absolute structure function. Nonetheless, we *still* find a very clear scaling of the absolute moments relative to each other. Here we would like to point to the experimental finding that it is the absolute third moment that is the correct moment to use in the scaling, not the third moment itself. The scaling constants agree surprisingly well with those obtained by other authors even at high Reynolds numbers. This hints that the relative scaling between the moments is not mediated by a indirect scaling with the third moment to τ, but is of an even more fundamental nature. Indeed one might speculate that the scaling properties usually attributed to fully developed turbulence are due to fundamental processes and effects also seen at low Reynolds numbers.

Although the corrective procedure found to work in the experiment may not be the correct to use in other cases we wish to stress that it seems possible experimentally to decide on which method to employ by using the above criterion and looking for extended self-similarity.

Due to the lack of analytic results many model distributions have been suggested as approximations to the real distributions for turbulent flows. In order to investigate the deviations from the Gaussian PDF, we have examined Gaussian-Lorentzian distribution. By rescaling u with respect to the second moment $\langle u^2 \rangle$, one parameter is eliminated, thus leaving a one-parameter family of Gaussian-Lorentzian distributions. A single parameter ν characterizes the form of the distribution. Our results show that the Gaussian-Lorentzian fit to experimental data works well within approximately 3 standard deviations from the mean but at higher values severely underestimates the tails of the distributions.

A remarkable fact is that the experimental moments, within experimental uncertainty, fall on unique curves, independent of Reynolds number, when using ν as parameter. This shows that the even part of the velocity difference distributions in terms of the rescaled velocity u' at least is very close to being a single-parameter family of distributions with second moment equal unity, although not the Gaussian-Lorentzian family.

One of us (PA) acknowledge financial support from the Novo-Nordisk Foundation.

References

1. P. Buchhave, W.K. Georg Jr, J.L. Lumley, Ann. Rev. Fluid Mech. **11**, 443 (1979).
2. D. Durox, T. Baritaud, Dantec Information **4** (1987).
3. D.A. Johnson, D. Modaress, F.K. Owen, J. Fluids Eng. **106**, 5 (1984).
4. R.V. Edwards, J. Fluids Eng. **109**, 89 (1987).
5. W. Fuchs, H. Albrecht, H. Nobach, C. Tropea, L.J.W. Graham, Proc. 6th Int. Symp. on Appl. of Laser Anemometry to Fluid Mech. (Lisbon 1992, Ladoan-Instituto Superior Technico Lisbon, Portugal) p 8.2.1.
6. A.R. Winter, L.J.W. Graham, K. Bremhorst, Exp. Fluids **11**, 147 (1991).
7. Do Hwan Lee, Exp. Fluids **16**, 223 (1994).
8. A.N. Kolmogorov, Dokl. Akad. Nauk. SSSR **30**, 301 (1941).
9. R. Benzi, S. Ciliberto, R. Tripiccione, C. Baudet, S. Succi, Phys. Rev. E **48**, R29 (1993); R. Benzi, S. Ciliberto, C. Baudet, G.R. Chavarria, R. Tripiccione, Europhys. Lett. **24**, 275 (1993). R. Benzi, S. Ciliberto, C. Baudet, G.R. Chavarria, Physica D **80**, 385 (1995).
10. S. Grossman, D. Lohse, A. Reeh, Phys. Rev. E **56**, 5473 (1997).
11. A.M. Obukhov, J. Fluid Mech. **13**, 77 (1962).
12. A.N. Kolmogorov, J. Fluid Mech. **13**, 82 (1962).
13. R.H. Kraichnan, Fluid Mech. **62**, 305 (1974).
14. B.B. Mandelbrot, J. Fluid Mech. **62**, (1974) 331.
15. B. Castaing, Y. Gagne, E.J. Hopfinger, Physica D **46**, 177 (1990).
16. C. Meneveau K.R. Sreenivasan, J. Fluid Mech. **224**, 429 (1991).
17. C. Beck, Phys. Rev. E **49**, 3641 (1994).
18. U. Frisch, *Turbulence: The Legacy of A.N. Kolmogorov* (Cambridge, 1996).
19. H.K. Pak, W.I. Goldburg, Phys. Rev. Lett. **68**, 938 (1992).
20. L.D. Landau, E.M. Lifshitz, *Fluid Mechanics*, 2nd edn., in Course of Theoretical Physics (Pergamon Press, 1987).
21. L.E. Drain, *Laser Doppler Anemometry* (John Wiley, 1980).
22. This will often be a good approximation in liquids, where Stokes law will limit gravitional effects and Brownian motion. In air the situation is more difficult and it is often a problem to seed the flow in a uniform way.
23. D.K. McLaughlin, W.G. Tiederman, Phys. Fluids **16**, 2082 (1973).
24. W.G. Tiederman, paper presented at 5th Biennal Symposium on Turbulence, Oct. 1977, Univ. Missouri, Rolla.
25. F. Esposito, E. Nino, C. Serio, Europhys. Lett. **35**, 653-658 (1996).
26. F. Anselmet, Y. Gagne, E. Hopfinger, R.A. Antonia, J. Fluid. Mech. **140**, 63 (1984).
27. See *e.g.* I.S. Gradstein, I.M. Ryzhik, *Table of Integrals and Products* (Academic Press, 1980).
28. For a complete derivation and some analytical results on moments see: Jesper Borg, internal report, NBI.